DOI: 10.1002/chem.200701471

Tuning the Magnetic Properties of $Li_xCrTi_{0.25}Se_2$ ($0.03 \leq x \leq 0.7$) by Directed Deintercalation of Lithium

Malte Behrens, Joseph Wontcheu, Ragnar Kiebach, and Wolfgang Bensch*[a]

Abstract: X-ray diffraction (XRD), in situ energy-dispersive X-ray diffraction (EDXRD), X-ray absorption near-edge structure (XANES), extended X-ray absorption fine structure (EXAFS), and magnetic measurements were applied to investigate the effects of lithium deintercalation on pseudolayered $Li_{0.70}CrTi_{0.25}Se_2$. A detailed picture of structural changes during the deintercalation process was obtained by combining the results of EDXRD and EXAFS. Removal of Li from the host–guest complex leads to anisotropic contraction of the unit cell with stronger impact on the *c* axis, which is the stacking axis of the layers. The EDXRD experiments evidence that the shrinkage of the lattice parameters with decreasing x_{Li} in $Li_xCrTi_{0.25}Se_2$ is nonlinear in the beginning and then becomes linear. Analysis of the EXAFS spectra clearly shows that the Cr/Ti–Se distances are affected in a different manner by Li removal. The Cr–Se bond lengths decrease, whereas the Ti–Se bonds lengthen when the Li content is reduced, which is consistent with XRD data. Magnetic measurements reveal a change from predominantly antiferromagnetic exchange ($\theta_p = -300$ K) interactions for the pristine material to ferromagnetic exchange interactions ($\theta =$ 25 K) for the fully intercalated material. Thus, the magnetic properties can be altered under ambient conditions by directed adjustment of the dominant magnetic exchange. The unusual magnetic behavior can be explained on the basis of the variation of the metal–metal distances and the Cr-Se-Cr angles with *x*, which were determined by Rietveld refinements. Owing to competing ferromagnetic and antiferromagnetic exchange interactions and disorder, the magnetic ground state of the intercalated materials is characterized by spin-glass or spin-glass-like behavior.

Keywords: chalcogenides · chromium · EXAFS spectroscopy · intercalations · magnetic properties

Introduction

Intercalation chemistry has a long tradition as a soft chemical method for preparing metastable compounds and altering physicochemical properties of materials.[1–4] Chalcogenides have often been the focus of intercalation/deintercalation chemistry due to the promising physical properties that can be tuned by electron transfer from the guest to the host material, and vice versa. The most prominent compounds were the transition-metal dichalcogenides (TMDCs), especially in view of the excellent behavior of TiS_2 as a material for rechargeable Li batteries. Such $LiTiS_2$ batteries permitted a deep cycling with about 1000 cycles and a very low capacity loss of less than 0.05%. However, intercalation is not only restricted to Li as guest species, and complex transition-metal chalcogenides such as $Tl_xV_5S_8$,[5,6] $Tl_xCr_5S_8$,[7] $K_{0.52}Ti_6Se_8$,[8] $Tl_xV_6S_8$,[9] $In_{0.69}V_6S_8$,[10] $Tl_xCr_5Se_8$,[11] $A_xNb_3Q_4$ (Q = S, Se, Te, A = In, Tl, Li)[12] were investigated in the past with respect to changes of the electronic, magnetic, and structural properties as function of the guest species. Prominent examples are the Chevrel phases $A_xMo_6Q_8$ (A = Li, Ca, Eu, Pb, Cu, Sn, etc.; Q = S, Se) which cover a wide range of physical properties such as superconductivity, high ion mobility, magnetism, and thermoelectricity.[4,13,14,15] Nowadays, intercalation/insertion chemistry is mainly focused on the synthesis of new Li battery materials, solid electrolytes, and electrochromic devices based on different oxidic compounds, phosphates,[16–21] layered oxide sulfides,[22] and thiospinels.[23]

The intercalation chemistry and physical properties of binary TMDC materials can be enhanced by introducing magnetically active transition metal ions in an ordered way into the van der Waals gaps. The series of compounds $Cr_{5-y'}Ti_{y'}Se_8$ can be described as self-intercalated TMDCs

[a] Dr. M. Behrens, Dr. J. Wontcheu, Dr. R. Kiebach, Prof. Dr. W. Bensch
Institut für Anorganische Chemie
University of Kiel
Olshausenstrasse 40–60, 24098 Kiel (Germany)
Fax: (+49) 341-880-1520
E-mail: wbensch@ac.uni-kiel.de

wherein one-fourth of the free octahedral voids in the gaps are occupied by transition-metal ions, that is, the formula of the compounds can be written as $Cr_{1.25-y}Ti_ySe_2$. Generally, intercalation of alkali metals A in transition metal chalcogenides is accompanied by charge transfer,[24,26] so that electrons can be "titrated" into the host to control the crystallographic and electronic structure and possibly the physical properties. The compounds with composition $Cr_{1.25-y}Ti_ySe_2$ have free lattice sites to accommodate guests and accessible electronic states for the transferred electrons. Recently, we started to investigate Li intercalation of $Li_xCr_{1.25-y}Ti_ySe_2$ phases with the aim of understanding the fundamental reaction mechanisms and the structural changes. We previously demonstrated that insertion of Li under thermodynamic control into the vacant sites in the $Cr_{1.25-y}Ti_ySe_2$ phases leads to structural changes from monoclinic to trigonal symmetry.[27,28]

The structure of monoclinic Cr_5Se_8 with Se atoms in a distorted hexagonally packed arrangement[29,30] can be regarded as the archetype of the $Li_xCr_{1.25-y}Ti_ySe_2$ series. However, Cr_5Se_8 can only be prepared at high pressures and high temperatures due to instability of Cr^{4+} (d^2 configuration) in an Se environment. By replacing Cr atoms by Ti, which easily adopts the Ti^{4+} state (d^0 configuration), isostructural compounds such as $CrTi_{0.25}Se_2$[31] and $Cr_{0.75}Ti_{0.5}Se_2$[32] can be prepared from the elements under ambient pressure. Substitution is thus needed for the preparation of such Cr-rich chalcogenide hosts. An appealing aspect is that the electronic structure and the nature of the d electrons can be directly influenced by choosing the Ti/Cr ratio, which leads to different physical properties which can be further tuned by alkali metal intercalation reactions.[24,25]

Neutron diffraction experiments on the host materials revealed that Cr atoms reside mainly in the partially occupied metal atom layer and that Ti is distributed over the fully occupied layers.[28,29] Recently, we demonstrated that Li can easily be deintercalated from $Li_xCr_{1.25-y}Ti_ySe_2$ by treatment with water.[24,25] The structure responds with a contraction, but no switching back of the symmetry is observed. Here we describe the effect of Li content on the magnetic properties, which to the best of our knowledge is the first example of tuning the magnetic behavior of TMDC-like materials by lithium intercalation. X-ray diffraction (XRD) data and X-ray absorption fine structure (XAFS) analyses of $Li_xCrTi_{0.25}Se_2$ with different x values are also discussed.

Results and Discussion

Owing to the transition to trigonal symmetry, the intercalation reactions of monoclinic $CrTi_{0.25}Se_2$ yield biphased products for intermediate Li contents.[25] Because the symmetry change is not reversible, single-phase samples of trigonal $Li_xCrTi_{0.25}Se_2$ ($0.03 < x < 0.70$) can be obtained by deintercalation of phase-pure $Li_{0.70}CrTi_{0.25}Se_2$. In the following, we discuss the impact of deintercalation on the structure and the magnetic properties of $Li_xCrTi_{0.25}Se_2$.

The XRD powder patterns of the intercalated samples can be indexed on the basis of the trigonal space group $P\bar{3}m1$. In this space group all metal atom sites in the partially occupied metal atom layer are equivalent. The Cr atoms residing in these layers are well ordered in the host and are not assumed to be mobile. The real structure should therefore exhibit a larger cell, but no peaks indicating a superstructure could be found. The small basic cell (Figure 1a) was used as structural model in the Rietveld refinements, and all reflections could be explained (Figure 1b). This model is also used in the following discussion.

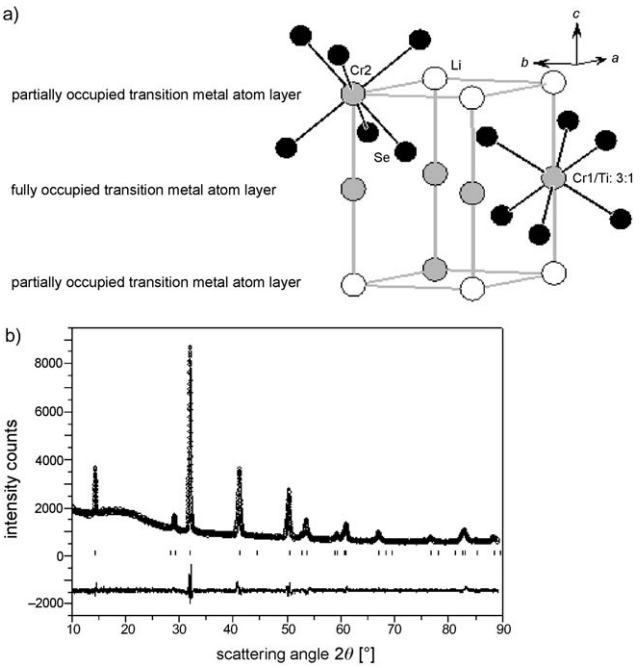

Figure 1. a) Crystal structure of $Li_xCrTi_{0.25}Se_2$; the trigonal cell was used as structural model for the Rietveld refinement of XRD powder data. Occupation of the partially occupied layers of transition metal atoms is in accordance with the monoclinic host material. The given transition metal distribution is as determined by neutron diffraction. b) Rietveld refinement of a fully intercalated sample $Li_{0.70}CrTi_{0.25}Se_2$ ($R_{Bragg} = 7.69\,\%$); the modulation of the background centered around $2\theta = 20°$ is due to the protective foil.

The lattice parameters of the trigonal materials contract as Li is deintercalated by treatment with water. In an in situ energy-dispersive X-ray diffraction (EDXRD) experiment, a shift of the peak positions to smaller d spacing (higher energies) was detected. The relative shifts of the three most intense reflections are depicted in Figure 2a. Clearly, most of the structural relaxation on deintercalation occurs within the first hour of reaction. Furthermore, the unit cell contracts in an anisotropic fashion.

Due to the low scattering power of Li, it usually cannot be detected by XRD. However, the increased electron density in the van der Waals gap of layered compounds derived from the CdI_2 structure type results in decreased intensity for the (001) reflection. Scattering centers in the void layers

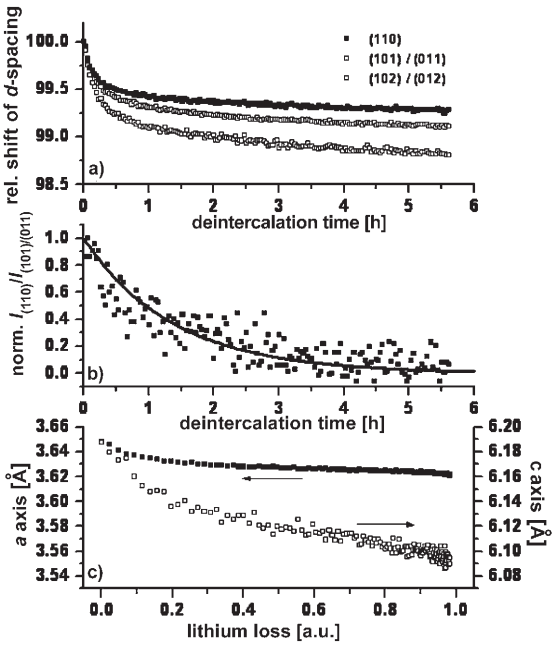

Figure 2. Relative shift of the *d* spacing of selected reflections of a $Li_{0.70}CrTi_{0.25}Se_2$ sample on deintercalation in water (a); evolution of the ratio of integral intensities of the (110) and the (101)/(011) reflections with time (b); and reduction of lattice parameters with Li removal (c). The composition of the sample at the end of the experiment was $Li_{0.24}CrTi_{0.25}Se_2$.

are located exactly halfway between the fully occupied layers and lead to partial destructive interference. Consequently, in NiAs and other compounds with fully and equally occupied layers, the (001) reflection is completely absent. The (101)/(011) reflections of $Li_xCrTi_{0.25}Se_2$ are analogously affected, whereas (110) is not, because the [110] direction is oriented parallel to the layers. Therefore, the ratio of the intensities of these two reflections is a measure of the electron density in the partially occupied layers and of the Li content in the samples. The evolution of $I_{(110)}/I_{(101)/(011)}$ with reaction time is shown in Figure 2b. The Li content decreases quickly in the beginning, but not as fast as the structural contraction of the host. The line in Figure 2b is the fit of an exponential decay to the data and was used as abscissa in Figure 2c, which displays the lattice parameters as a function of Li removal. The lengths of the axes were calculated from the *d* values of the (110) and the (101) reflections. Figure 2c shows that 1) the effect of Li removal on the axes is much more pronounced for the *c* axis than for the *a* axis, 2) contraction of the lattice parameters is strong and nonlinear for the first 20% of Li deintercalation, and 3) a linear relationship between the lattice parameters and the Li content exists for the rest of the reaction. The *c* axis is the stacking axis of the metal atom layers. A strong impact of intercalation/deintercalation on this axis was also observed in intercalated TMDCs A_xMQ_2 (A = alkali metal; M = metal of Groups 4–6; Q = S, Se, Te); this demonstrates the structural relationship between layered TMDCs and the pseudo-layered host $CrTi_{0.25}Se_2$. In intercalated TMDCs the variation of the *c* axis can be attributed to both geometric and electronic effects.[22] A considerable decrease in the *a* axis is also detected, and Δa is about 26% of Δc, which is significantly higher than found for A_xMQ_2 phases such as Li_xTiSe_2, in which $\Delta a/\Delta c$ is usually 10%. This suggests that pronounced structural rearrangements also occur within the fully occupied layers, most likely due to electronic reasons.

Comparison of the contraction of the *a* and *c* axes obtained from in situ measurements (EDXRD) with those from PXRD (Rietveld analyses) revealed a small difference. From the EDXRD data, the *a* and *c* axes contract from 3.65 to 3.62 Å and from 6.19 to 6.09 Å, respectively, in the concentration range 0.70–0.24, and the analogous values determined by Rietveld refinements are 3.622–3.598 Å and 6.14–6.02 Å. The relative changes of 0.8 and 0.7% are very similar. The differences in the absolute data can be understood by keeping in mind that only two reflections of the EDXRD data were used for estimating the lattice parameters. Furthermore, the alignment of the EDXRD setup is not as accurate as of a powder diffractometer. The EDXRD data show broad reflection profiles, and no correction of the zero point is possible with the setup used for the experiments. Therefore, the data evaluated from reflections of EDXRD patterns are less accurate than those of a Rietveld refinement of a whole powder pattern.

Due to the small difference in electron density, it is not possible to unambiguously discriminate Ti and Cr by XRD experiments. Therefore, element-specific XAFS spectroscopy was applied to check whether a difference in the structural environments around Cr and Ti exists and if different effects of the oxidation introduced by Li deintercalation can be observed for the two types of metal atoms. X-ray absorption near-edge structure (XANES) spectra, extended X-ray absorption fine-structure (EXAFS) oscillations, and Fourier-transformed EXAFS (FT-EXAFS) amplitudes for Cr and Ti K-edge data of $Li_xCrTi_{0.25}Se_2$ samples with $x = 0.2$ and 0.7 were recorded, and representative results are shown in Figure 3.

The similar XANES spectra for Ti and Cr mean that both transition metals reside in similar coordination environments. In the FT-EXAFS spectra only the first M–Se shell (M = Ti, Cr) can be detected. According to the crystallographic data, all transition metal atoms are in an octahedral environment of six Se atoms with equal M–Se distances in each cluster. In the trigonal structure two different $CrSe_6$ octahedra exist: 75% (Cr1) of the Cr atoms are located in the fully occupied transition-metal atom layers, and 25% (Cr2) together with Li in the partially occupied layers (see Figure 1a). The $Cr2Se_6$ units exhibit longer Cr–Se contacts than $Cr1Se_6$. Both $CrSe_6$ clusters were fitted simultaneously in *R* space with a fixed 1:3 ratio to the experimental Cr K-edge spectra. Titanium resides exclusively in the fully occupied metal atom layer, and a unique $TiSe_6$ cluster exists that was used as a model. Spectra of the host were recorded for comparison, and refinement was carried out with the same models as for the intercalated phases. The MSe_6 octahedra in the host are more strongly distorted due to the more

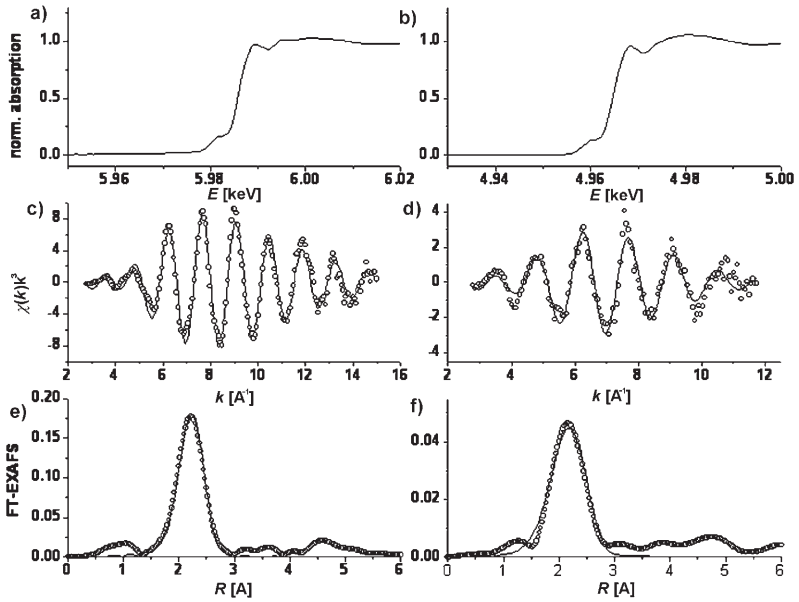

Figure 3. Representative XANES spectra (a, b), oscillations $\chi(k)$ (c, d; k^3-weighted EXAFS), and FT-EXAFS magnitudes (d, e; no correction for EXAFS phase shift) of a sample of the composition $Li_{0.2}CrTi_{0.25}Se_2$ recorded at the Cr K-edge (left column) and Ti K-edge (right column); data points in c)–f) represent the experiment; full lines are fits of theoretical data.

lar M–Se distances are found for the fully intercalated samples, but lowering the Li content increases the Ti–Se bond length, whereas the Cr1–Se distance is shortened. This different behavior of the intralayer M–Se distances with decreasing x is an electronic effect because geometric effects due to the presence of Li^+ would affect the atomic distances uniformly. A possible explanation is that oxidation on deintercalation occurs locally on the Cr1 centers to form smaller Cr^{III} ions from initially present Cr^{II}, whereas the removal of electrons from electronic states based on the Ti d band depletes the band and thus results in weaker interactions.

The magnetic properties of chromium chalcogenides are

Table 1. Results of EXAFS fits for different $Li_xCrTi_{0.25}Se_2$ samples with models for the coordination clusters derived from the crystallographic data.

	MSe_6	M–Se [Å]	D–W factor [Å^2]	E_0 shift [eV]
$CrTi_{0.25}Se_2$ [a]	$Cr1Se_6$ (75%)	2.522(1)	0.007096(1)	7.562(1) [b]
	$Cr2Se_6$ (25%)	2.627(1)	0.008078(1)	7.562(1) [b]
	$TiSe_6$ (100%)	2.544(1)	0.021017(1)	7.681(1)
$Li_{0.2}CrTi_{0.25}Se_2$	$Cr1Se_6$ (75%)	2.527(1)	0.006773(1)	7.421(1) [b]
	$Cr2Se_6$ (25%)	2.637(1)	0.008453(1)	7.421(1) [b]
	$TiSe_6$ (100%)	2.540(1)	0.017630(1)	7.393(1)
$Li_{0.7}CrTi_{0.25}Se_2$	$Cr1Se_6$ (75%)	2.531(1)	0.007215(1)	7.633(1) [b]
	$Cr2Se_6$ (25%)	2.667(1)	0.006415(1)	7.633(1) [b]
	$TiSe_6$ (100%)	2.539(1)	0.023521(1)	7.346(1)

[a] Monoclinic host $CrTi_{0.25}Se_2$ prior to phase transition. [b] E_0 shifts of each Cr K-edge spectrum were correlated during the fitting procedure of the two CrSe clusters.

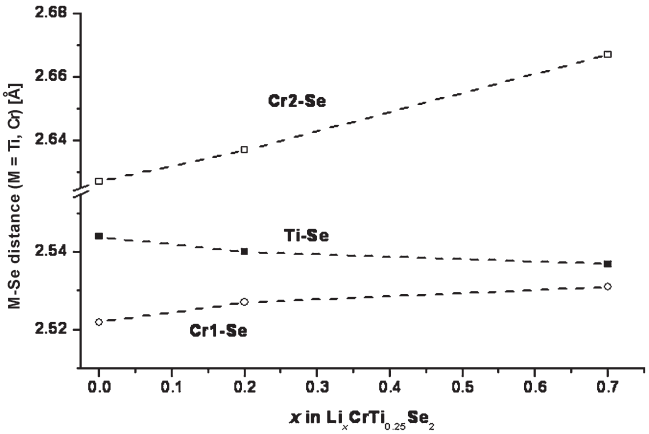

Figure 4. M–Se distances as obtained from EXAFS fits for $Li_xCrTi_{0.25}Se_2$ samples with different x; dashed lines are guides for the eye.

complex monoclinic structure. Different M–Se distances are present within each shell, and the applied models thus oversimplify the picture. However, using the monoclinic crystallographic data as model would result in too many independent parameters for the refinement to give reliable data. Nevertheless, reasonable fits are obtained with the simple models, and the reported M–Se distances refer to average values. Results of the EXAFS fits are compiled in Table 1; distance data are shown in Figure 4.

The Cr2–Se distance decreases with decreasing Li content. This trend is in agreement with results of Rietveld refinement of XRD powder data and is due to the contraction of the interlayer spacing as Li leaves the sites in the partially occupied metal atom layer. In the fully occupied layer, simi-

governed by the exchange interaction between neighboring Cr centers and are influenced by the structural rearrangement observed on Li deintercalation. A detailed discussion of the magnetic properties of the monoclinic host material including a description of the spin-glass behavior at low temperatures was given recently.[28] The host is paramagnetic in the high temperature range (>300 K) with a magnetic moment of 4.01 μ_B, which is larger than the spin-only value for Cr^{III}. However, such large magnetic moments have often been observed in chromium(III) chalcogenides. The susceptibility follows a Curie–Weiss law with a Weiss constant of about −300 K that indicates dominant antiferromagnetic exchange interactions.

The reciprocal magnetic susceptibilities for representative intercalated samples of batch I are shown in Figure 5. The slope of all curves is very similar in the high-temperature region, and similar effective magnetic moments were obtained on fitting the data to the Curie–Weiss law (Table 2).

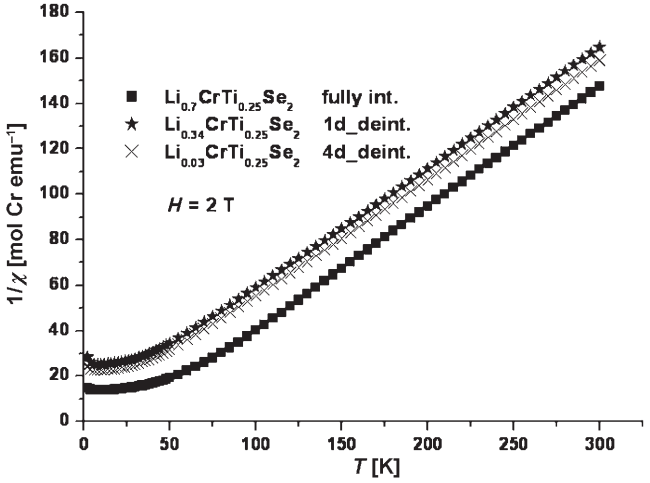

Figure 5. Reciprocal susceptibility as a function of temperature (2–300 K) for $Li_xCrTi_{0.25}Se_2$ samples with x = 0.7, 0.34, and 0.03.

Table 2. Magnetic data of the pristine material and of representative $Li_xCrTi_{0.25}Se$ samples.

	μ_{eff} [μ_B/Cr]	θ_p [K]
Batch I		
$CrTi_{0.25}Se_2$[a]	4.1	−300
$Li_{0.7}CrTi_{0.25}Se_2$	3.85	25
$Li_{0.34}CrTi_{0.25}Se_2$	3.92	−5
$Li_{0.03}CrTi_{0.25}Se_2$	3.88	−10
Batch II		
$CrTi_{0.25}Se_2$[b]	4.00(8)	−305(5)
$Li_{0.7}CrTi_{0.25}Se_2$	3.90(2)	61(2)
$Li_{0.48}CrTi_{0.25}Se_2$	3.92(3)	−11(2)
$Li_{0.24}CrTi_{0.25}Se_2$	3.87(3)	−47(1)

[a] Data from ref. [28], fitting range: 300–600 K; fitting range of all other samples: 100–300 K. [b] Fitting range: 200–340 K; for all other samples: 80–340 K.

If only Cr atoms are considered, they are 3.85, 3.92 and 3.88 μ_B for $Li_{0.7}CrTi_{0.25}Se_2$, $Li_{0.34}CrTi_{0.25}Se_2$, and $Li_{0.03}CrTi_{0.25}Se_2$, respectively. Theoretical magnetic moments calculated for different possible electronic situations hardly differ. For example, the magnetic moments of $(Li^+)_{0.34}(Cr^{3+})(Ti^{2+})_{0.25}(Se^{2-})_2$ and $(Li^+)_{0.34}(Cr^{3+})_{0.75}(Cr^{2+})_{0.25}(Ti^{3+})_{0.25}(Se^{2-})_2$ vary only by roughly 0.1 μ_B. Temperature-independent Pauli paramagnetism of potentially delocalized Ti levels further complicates the situation. Consequently, no reliable conclusion concerning the redox chemistry can be drawn from these data.

A linear behavior of the reciprocal susceptibility is observed for the intercalated samples in the temperature range 100–300 K, that is, the broad susceptibility maximum observed for the host in this temperature range is absent. The Weiss constant of 25(1) K for the fully intercalated sample of batch I indicates predominately ferromagnetic exchange interactions. Weiss constants of −5(1) and −10(1) K were found for $Li_{0.34}CrTi_{0.25}Se_2$ and $Li_{0.03}CrTi_{0.25}Se_2$, respectively (see Table 2), that is, ferromagnetic exchange is weakened when lithium is removed from $Li_xCrTi_{0.25}Se_2$. The magnetic data for samples of batch II (Table 2) demonstrate the influence of a slightly differing Cr content. For the intercalated materials the Weiss constant ranges from −47 K for $x = 0.24$ to 61 K for $x = 0.70$.

In the Li poorest material antiferromagnetic exchange is much weaker than for the pristine material. This drastic change cannot be explained on the basis of the small electron transfer in $Li_{0.03}CrTi_{0.25}Se_2$, but must be rather due to the structural alterations introduced by the structural phase transition. The results of the magnetic measurements can be understood on the basis of the Goodenough–Kanamori rules.[33,36] Direct antiferromagnetic exchange is expected for neighboring Cr atoms if their separation is less than about 3.5 Å. This is the case in the pristine material for the interlayer Cr−Cr contacts (face-sharing $CrSe_6$ octahedra, Table 3, Figure 6), and a large negative Weiss constant results.

Table 3. M–M distances from Rietveld refinement of powder patterns of a series of $Li_xCrTi_{0.25}Se_2$ samples with different x obtained by deintercalation in water for different times t.

	t [h]	Cr1/Ti–Cr1/Ti [Å]	Cr1/Ti1–Cr2 [Å]	R_{Bragg} [%]
$CrTi_{0.25}Se_2$[a]	–	3.460(1)[b]	3.006(1)[b]	4.61[c]
$Li_{0.03}CrTi_{0.25}Se_2$	96	3.510(1)	3.004(5)	7.18
$Li_{0.24}CrTi_{0.25}Se_2$	36	3.597(3)	3.010(1)	8.51
$Li_{0.34}CrTi_{0.25}Se_2$	24	3.598(1)	3.011(5)	5.62
$Li_{0.48}CrTi_{0.25}Se_2$	12	3.614(2)	3.056(6)	6.36
$Li_{0.7}CrTi_{0.25}Se_2$	0	3.622(8)	3.070(8)	7.69

[a] Monoclinic host $CrTi_{0.25}Se_2$ prior to phase transition. [b] Average distance obtained from the single-crystal structure determination of the monoclinic host $CrTi_{0.25}Se_2$[28]. [c] wR_2 of the single-crystal structure determination for 619 reflections with $F_0 > 4\sigma(F_0)$.

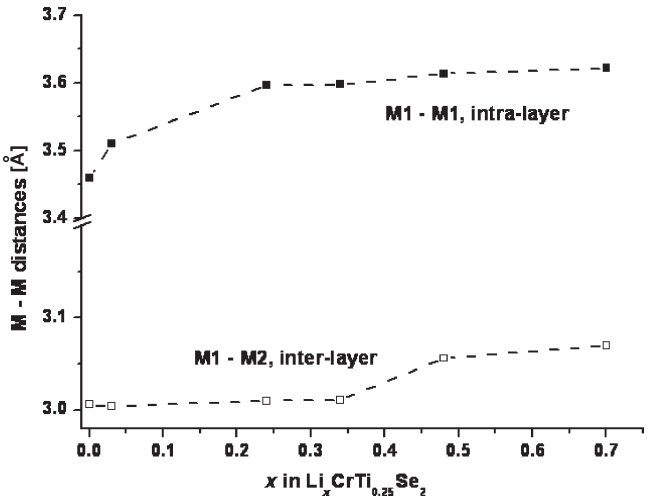

Figure 6. M−M distances in $Li_xCrTi_{0.25}Se_2$ samples with different x, as obtained by Rietveld refinement (M = Cr, Ti) of XRD powder patterns; The M1−M1 spacing is equal to the trigonal a axis, and two M1−Cr2 distances correspond to the c axis; dashed lines are guides for the eye.

The Cr–Cr distances in the fully occupied metal atom layers are significantly longer, and superexchange of the type Cr-Se-Cr must be invoked, which is of ferromagnetic nature. However, the Cr-Se-Cr angles significantly deviate from 90°, so that the ferromagnetic exchange interaction is weak. In the intercalated samples the intralayer M–M distances are longer than 3.5 Å, and ferromagnetic superexchange interactions via Cr-Se-Cr angles which are now 90° dominate in the fully occupied layers of transition metal atoms. On the other hand, antiferromagnetic interlayer exchange interactions are present via Cr1–Cr2 contacts, which remain well below 3.1 Å in all samples. In the sample with $x=0.03$ these distances are near the value of the genuine material and obviously the antiferromagnetic interaction dominates. Therefore, negative values for θ_p are still observed for this sample. The fully intercalated sample $Li_{0.70}CrTi_{0.25}Se_2$ has the largest Cr1–Cr1 distance, and consequently ferromagnetic intralayer exchange interactions are stronger than antiferromagnetic exchange, and a positive Weiss constant results. If the electrons are transferred from Li to localized Cr d states Cr^{II} and Cr^{III} coexist, and Zener double-exchange between Cr atoms sharing common faces, which is ferromagnetic, must be considered. In summary, the pronounced changes in magnetic behavior on Li intercalation are an interplay of geometric and electronic effects. The saturation magnetization experiment performed at 10 K for $Li_{0.70}CrTi_{0.25}Se_2$ (Figure 7) shows that the material behaves like a soft ferromagnet with a low value of the coercive field (0.03 T) and a small value of the remanence field strength of about 0.15 emu g^{-1}. Note that even at 9 T no saturation is observed, which is an indication of the spin-glass-like behavior of the material.

The dc magnetization M with different applied fields of three intercalated samples of batch I are displayed in Figure 8. The M value exhibits pronounced irreversibility for all materials, indicated by the divergence of the field-cooled (M_{fc}) and zero-field-cooled (M_{zfc}) magnetization curves below a distinct temperature T_f. The splitting shifts to lower temperatures as H increases, and the irreversibility between the M_{zfc} and M_{fc} curves is clearly reduced. These two observations are further hints for spin-glass or spin-glasslike behavior. Interestingly, the M_{fc} curves for $T<T_f$ slightly level off with decreasing T, similar to the behavior observed in canonical spin glasses.[37] The compounds exhibit structural disorder and competing ferromagnetic and antiferromagnetic exchange interactions, which are a prerequisites for the occurrence of spin-glass behavior. Because the conductivity of the compounds as function of Li content is not known, the occurrence of the spin-glass behavior due to the Ruderman–Kittel–Kasuya–Yosida (RKKY) mechanism cannot be ruled out. The nature of the divergence of the M_{zfc} and M_{fc} curves was further investigated with ac susceptibility measurements, and an example of the frequency dependence of χ' and χ'' for $Li_{0.7}CrTi_{0.25}Se_2$ is shown in Figure 9. The freezing temperature T_f in the χ' curve shows a shift to higher temperatures with increasing applied frequency, from 40.6 K for 30 Hz to about 42 K for 1000 Hz. A pronounced shift is also observed in the χ'' curve from 31 K (30 Hz) to 34.7 K (1000 Hz). The frequency-dependent shift of the freezing temperature is a typical behavior of spin-glasses.

Conclusion

We have demonstrated that Li intercalation/deintercalation is a powerful synthetic approach to tune the magnetic properties of $Li_xCrTi_{0.25}Se_2$ under ambient conditions. The structural response of the complex pseudolayered $Li_xCrTi_{0.25}Se_2$ system to the removal of Li from the host–guest complex is 1) a more or less linear contraction of the unit-cell volume caused predominantly by contraction along the stacking axis of the layers; 2) electronically driven rearrangement of interatomic bonding within the fully occupied layers, which features an increase in the Ti–Se distance; and 3) shortening of the M–M bond lengths, which is more pronounced for intralayer contacts and less strong for interlayer distances, so that the latter almost reach the value observed for the host, whereas the former do not. Alteration of the M–M distances and M-Se-M angles leads to a change from predominantly antiferromagnetic exchange interactions for the pristine material to dominant ferromagnetic interactions for the fully intercalated material, which originate from superexchange in the fully occupied layers. Even for the sample with the lowest Li content, the strong antiferromagnetic exchange present in the pristine material is not achieved. This observation can only be explained on the basis of differing magnetic exchange

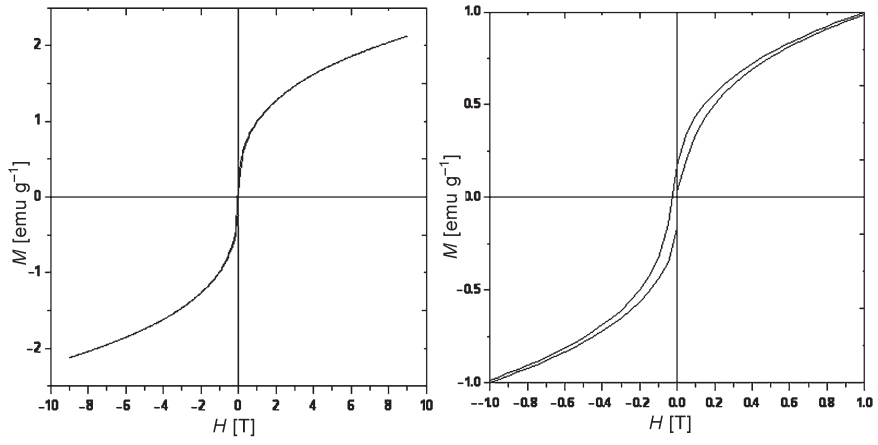

Figure 7. Field-dependent magnetization for $Li_{0.70}CrTi_{0.25}Se_2$ at 10 K (left) and enlarged view (right). Note that the full hysteresis loop was not measured.

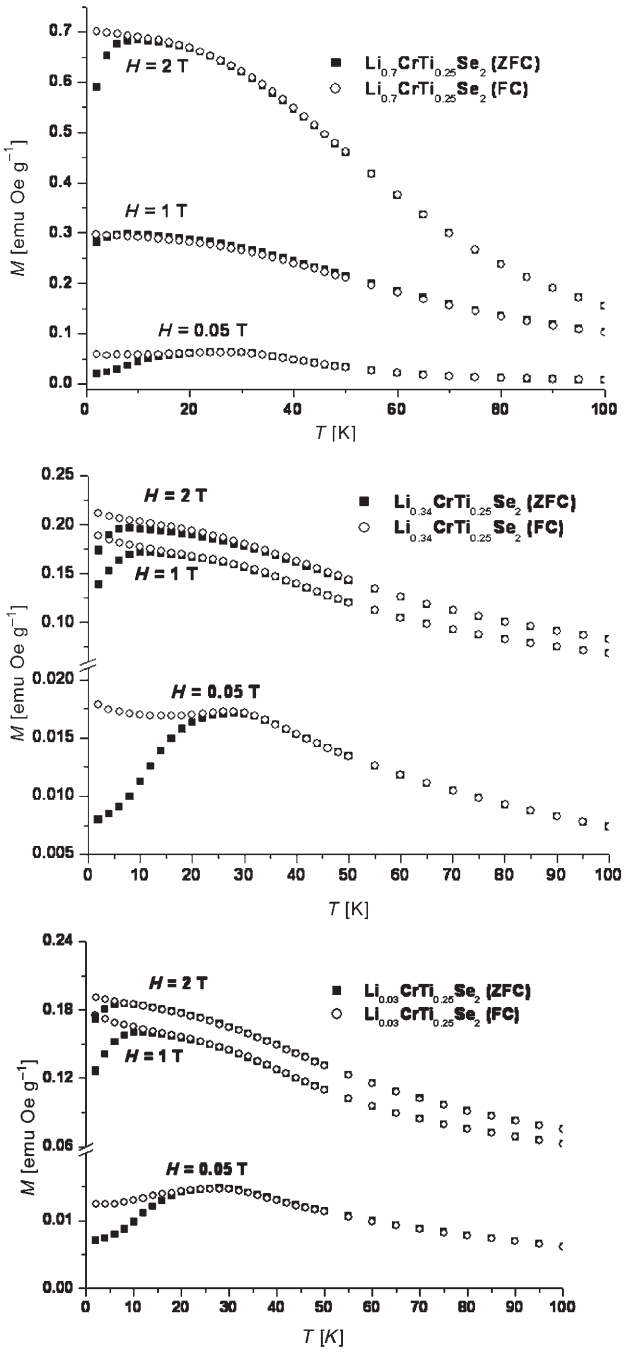

Figure 8. M_{fc} (open circles) and M_{zfc} (filled squares) for representative $Li_xCrTi_{0.25}Se_2$. Top: $Li_{0.7}CrTi_{0.25}Se_2$, middle: $Li_{0.34}CrTi_{0.25}Se_2$, and bottom: $Li_{0.03}CrTi_{0.25}Se_2$ with applied fields of 0.05, 1, and 2 T.

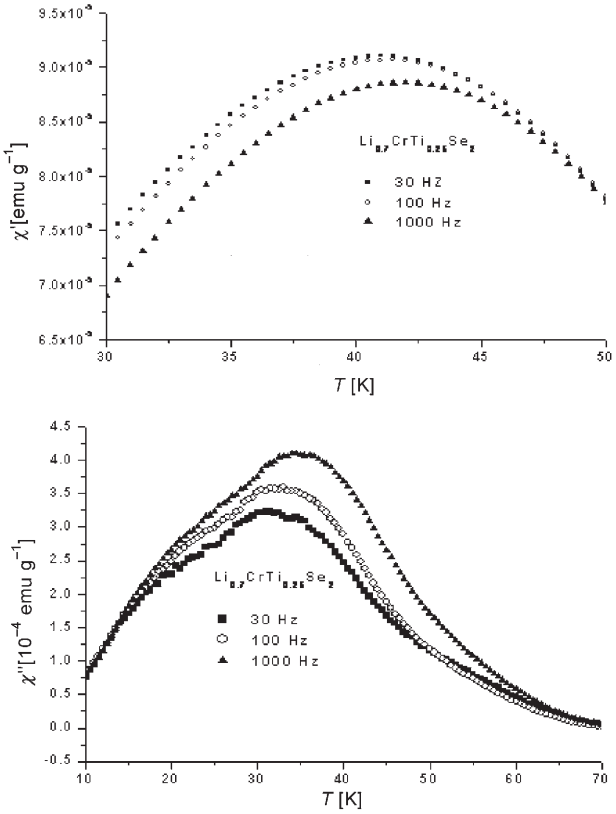

Figure 9. Frequency dependence of real part (χ'; top) and imaginary part (χ''; bottom) in the region of the freezing temperature T_f, determined by ac measurements on $Li_{0.7}CrTi_{0.25}Se_2$.

interactions between the two materials due to an altered bonding situation. The magnetic ground state of intercalated samples is characterized by spin-glass-like behavior. The present results encourage studies on further magnetic TMDC-like materials or other magnetic compounds that allow insertion of Li due to suitable structural and electronic features. Furthermore, Li intercalation with simultaneous electron transfer calls for further investigation of the ionic and electronic conductivity of the different materials. Compounds showing both types of conductivity are promising as electrode materials in Li batteries.

Experimental Section

To perform all experiments presented here two batches of $CrTi_{0.25}Se_2$ were prepared from the elements in evacuated silica ampoules (950 °C, 10 days). The chemical composition of the samples was first verified by EDX analysis. The average composition of batch I was $Cr_{1.03(1)}Ti_{0.26(2)}Se_2$ with standard deviations estimated on the basis of the number of analyses. This batch was used for the full characterization of the magnetic properties of intercalated samples in the high- and low-temperature regions. Batch II with composition $Cr_{1.07(1)}Ti_{0.23(1)}Se_2$ was used for the EXAFS and in situ X-ray scattering experiments. In addition, the magnetic properties of intercalated materials of this batch were investigated in the high-temperature region (see below).

Finally, the compositions were confirmed by means of inductively coupled plasma (ICP) and atomic absorption spectroscopy (AAS) analysis with an accuracy of about 2%. The Li content of intercalated samples was determined by AAS (Perkin-Elmer AAnalyst 300). For this purpose, a fraction of the samples was dissolved in HNO_3 (65%) and H_2O_2 (30%) and the Li and Se contents of the solution were determined to calculate x in $Li_xCrTi_{0.25}Se_2$. (AAS accuracy is typically 0.4%). The pristine material was obtained as a gray powder with platelike crystallites of sizes ranging from 2 to 15 μm. Phase pureness was checked by Rietveld refinement of XRD powder patterns recorded on a STOE Stadi-P diffractometer ($Cu_{K\alpha}$ radiation, Ge monochromator, linear PSD, 2θ range: 10–90°, step

width: 0.01°, step time: around 1 h) for the concentration range $x = 0.70$–0.03. The R_{Bragg} values were better than 8.5% for all samples. For refinement the program package Fullprof[38] was used: Thompson–Cox–Hastings pseudo-Voigt profiles, extrapolation of background from manually selected points, preferred orientation modeled with March–Dollase function, zero point as global parameter.

The host $CrTi_{0.25}Se_2$ was chemically intercalated by suspending the powder in a solution of *n*-butyllithium in an Ar glove box. Thick-walled sealable test tubes were used as reaction vessels and heated to 60 °C (typical reaction: 50 mg of $CrTi_{0.25}Se_2$, 5 mL of 1.6 M *n*BuLi in hexane). After about 3 days the powder was collected by filtration and washed with hexane. XRD patterns were recorded to check completeness of the phase transition. The sample holder was sealed with X-ray-transparent foil to protect the samples from air and moisture.

Fully intercalated samples were transferred from the glove box and treated with doubly distilled water for deintercalation. After certain reaction times, samples were collected, filtered, washed with water and ethanol, dried, and characterized by XRD and AAS. Without ultrasonication the minimal x was 0.20, whereas samples with $x \approx 0.03$ can be prepared with ultrasonication.

EXAFS spectra at the Ti and Cr K-edges were recorded at the E4 beamline of HASYLAB, Hamburg, Germany, in transmission geometry using a double Si single-crystal monochromator and ionization chambers. For this purpose, the samples were thoroughly ground with cellulose and pressed into pellets. Cr and Ti foils were used as reference for the energy scale and measured simultaneously with the intercalated samples. Spectra were evaluated with the software WinXAS[39] and FEFF 8.2.[40] Theoretical spectra were calculated by using crystallographic data as models for the coordination clusters around the absorber atoms and fitted to experiment to elucidate structural information. The S_0^2 parameter (0.9) and the coordination number of the MSe_6 clusters were fixed during refinement.

One sample of intercalated material was studied by in situ energy-dispersive XRD (in situ EDXRD). It was suspended in water (2 mL) and stirred. During the deintercalation process powder patterns of the suspension were recorded every 2 min with synchrotron radiation at beamline F3 at HASYLAB for the concentration range $x = 0.70$–0.24. The intensity of the white beam is sufficient to penetrate through the test tube walls, and diffracted intensity was recorded at a distinct angle with an energy-dispersive detector.[41]

Magnetic measurements on intercalated samples of batch II were done between 77 and 340 K on a Faraday balance applying a field of 1.5 T. The samples of batch I were characterized with a PPMS magnetometer. Samples were loaded into gelatine capsules inside an argon-filled glove box and immediately transferred to the magnetometer to avoid reaction of the materials with air and moisture. The dc susceptibilities were measured in the temperature range of $2 \le T \le 300$ K with a field of 2 T. The zero-field-cooled and field-cooled magnetizations M_{zfc} and M_{fc} were taken as follows. The system was cooled in zero field to 2 K, a field of 0.05, 1, or 2 T set immediately after $T = 2$ K was reached, and M_{zfc} data were taken on warming from 2 to 100 K; M_{fc} data were recorded on cooling from 100 to 2 K. The ac susceptibilities were measured for the fully intercalated sample $Li_{0.7}CrTi_{0.25}Se_2$ with a PPMS magnetometer in an applied field of 5 Oe at 30, 100, and 1000 Hz. Field-dependent magnetizations were recorded at 10.0 K with a field of up to 9 T.

Acknowledgements

We thank HASYLAB, DESY for the allocation of synchrotron measurement time. The financial support of the State of Schleswig-Holstein and the Deutsche Forschungsgemeinschaft (DFG, SPP 1136) is acknowledged.

[1] *Progress in Intercalation Research* (Eds.: W. Müller-Warmuth, R. Schöllhorn), Kluwer, Dordrecht, **1994**.
[2] *Intercalated Layered Materials* (Ed.: F. A. Levy), D. Reidel Publishing Company, Dordrecht, **1979**.
[3] *Handbook of Nanostructured Materials and Nanotechnology* (Ed.: H. S. Nalwa), Academic Press, San Diego, **2000**.
[4] R. Schöllhorn, *Phys. Intercal. Comp. Conf.*, Trieste, **1981**, p. 33; R. Schöllhorn, *Angew. Chem.* **1980**, *92*, 1015–1035; *Angew. Chem. Int. Ed. Engl.* **1980**, *19*, 983–1003; R. Schöllhorn, *Pure Appl. Chem.* **1984**, *56* 1739–1752.
[5] W. Bensch, E. Wörner, M. Muhler, U. Ruschewitz, *Eur. J. Solid State Inorg. Chem.* **1993** *30*, 645–658.
[6] T. Ohtani. S. Onoue, *Mater. Res. Bull.* **1986**, *21*, 69–76.
[7] W. Bensch, E. Wörner, M. Muhler, U. Ruschewitz, *J. Solid State Chem.* **1994**, *110*, 234–242.
[8] W. Bensch, J. Koy, T. Braun, P. Hug, *Solid State Ionics* **1994**, *74*, 141–148.
[9] H. Eckert, W. Müller-Warmuth, W. Schramm. R. Schöllhorn, *Solid State Ionics* **1984**, *13*, 1–6; W. Bensch, J. Koy, W. Biberacher, *Solid State Commun.* **1995**, *93*, 261–264.
[10] W. Bensch, J. Koy, W. Biberacher, *Mater. Res. Bull.* **1995**, *30*, 1217–1226.
[11] W. Bensch, O. Helmer, C. Näther, *J. Solid State Chem.* **1996**, *127*, 40–50; W. Bensch, O. Helmer, M. Muhler, *J. Alloys Compd.* **1997**, *246*, 62–69; T. Ohtani, Y. Sano, K. Kodama, S. Onoue, H. Nishihara, *Mater. Res. Bull.* **1993**, *28*, 501–508.
[12] T. Ohtani, Y. Sano, Y. Yokota, *J. Solid State Chem.* **1993**, *103*, 504–513; G. Huan, M. Greenblatt, *Mater. Res. Bull.* **1987**, *22*, 943–949; K. Sakai, Y. Ishihara, H. Okamoto, K. Tsutsumi, H.-Z. Lu, *Solid State Commun.* **1991**, *77*, 73–76; F. W. Boswell, J. C. Bennett, *Mater. Res. Bull.* **1996**, *31*, 1083–1092; T. Ohtani, Y. Yokota, H. Sawada, *Jpn. J. Appl. Phys.* **1999**, *38*, L142L144.
[13] R. Chevrel, M. Sergent in *Topics of Current Physics, Superconductivity in Ternary Compounds I, Vol. 32* (Eds.: O. Fischer, M. B. Maple), Springer, Berlin, **1982**.
[14] T. Caillat, J.-P. Fleurial, G. J. Snyder, *Solid State Sci.* **1999**, *1*, 535–544.
[15] M. A. McGuire, A. M. Schmidt, F. Gascoin, G. J. Snyder, F. J. DiSalvo, *J. Solid State Chem.* **2006**, *179*, 2158–2163.
[16] M. S. Whittingham, *Chem. Rev.* **2004**, *104*, 4271–4301.
[17] M. S. Whittingham, *Solid State Ionics* **2000**, *134*, 169–178.
[18] M. S. Whittingham, Y. Song, S. Lutta, P. Y. Zavalij, N. A. Chernova, *J. Mater. Chem.* **2005**, *15*, 3362–3379.
[19] J.-M. Tarascon, M. Armand, *Nature* **2001**, *414*, 359–367.
[20] A. D. Robertson, A. R. West, A. G. Ritchie, *Solid State Ionics* **1997**, 104, 1–11.
[21] G. A. Adachi, N. Imanaka, H. Aono, *Adv. Mater.* **1996**, *8*, 127–135.
[22] S. Indris, J. Cabana, O. J. Rutt, S. J. Clarke, C. P. Grey, *J. Am. Chem. Soc.* **2006**, *128*, 13354–13355; O. J. Rutt, T. L. Hill, Z. A. Gal, M. A. Hayward, S. J. Clarke, *Inorg. Chem.* 2003, 42, 7906–7911.
[23] V. Bodenez, L. Dupont, M. Morcrette, C. Surcin, D. W. Murphy, J.-M. Tarascon, *Chem. Mater.* **2006**, *18*, 4278–4287.
[24] R. Schöllhorn, *Angew. Chem.* **1980**, *92*, 477–478; *Angew. Chem. Int. Ed. Engl.* **1980**, *19*, 983–1003.
[25] J. Rouxel, *J. Chim. Phys. Phys.-Chim. Biol.* **1986**, *83*, 841–850.
[26] M. S. Whittingham, *Prog. Solid State. Chem.* **1978**, *12*, 41–99.
[27] J. Wontcheu, M. Behrens W. Bensch, S. Indris, M. Wilkening, P. Heitjans, *Solid State Ionics* **2007**, *178*, 759–768.
[28] M. Behrens, O. Riemenschneider, W. Bensch, S. Indris, M. Wilkening, P. Heitjans, *Chem. Mater.* **2006**, *18*, 1569–1576.
[29] A. W. Sleight, T. A. Bither, *Inorg. Chem.* **1969**, *8*, 566–569.
[30] H. Huppertz, H. Lühmann, W. Bensch, *Z. Naturforsch B* **2003**, *58*, 934–938.
[31] W. Bensch, B. Sander, C. Näther, R. K. Kremer, C. Ritter, *Solid State Sci.* **2001**, *3*, 559–568.
[32] J. Wontcheu, W. Kockelmann, Zh.-L. Huang, W. Schnelle, W. Bensch, *Solid State Sci.* **2007**, *9*, 506–514.
[33] J. B. Goodenough, *J. Phys. Chem. Solids* **1958**, *6*, 287–297.
[34] J. B. Goodenough, *Phys. Rev.* **1955**, *100*, 564–573.
[35] J. Kanamori, *J. Phys. Chem. Solids* **1959**, *10*, 87–98.
[36] J. B. Goodenough, *J. Phys. Chem. Solids* **1969**, *30*, 261–280.

[37] J. A. Mydosh, *Spin Glasses: An Experimental Introduction* (Taylor & Francis, London) **1993**, p. 87.
[38] J. Rodriguez-Carvajal, FULLPROF, Lab. Leon Brillouin, Gif-sur-Yvette Cedex (France), **2005**.
[39] T. Ressler, WinXAS 3.1, **2004**.
[40] A. L. Ankudinov, B. Ravel, J. J. Rehr, S. D. Conradson, *Phys. Rev. B* **1998**, *58*, 7565–7576.
[41] L. Engelke, M. Schaefer, M. Schur, W. Bensch, *Chem. Mater.* **2001**, *13*, 1383–1390.

Received: September 17, 2007
Revised: February 18, 2008
Published online: April 16, 2008

